ARTICLE

OPEN

Check for updates

Skillful multiyear to decadal predictions of sea level in the North Atlantic Ocean and U.S. East Coast

Liping Zhang [1,2 ✉], Thomas L. Delworth [1], Xiaosong Yang [1] & Fanrong Zeng[1]

Long-term sea-level rise and multiyear to decadal sea level variations pose substantial risks for flooding and erosion in coastal communities. Here we use observations and climate model predictions to show that sea level variations along the U.S. East Coast are skillfully predictable 3 to 10 years in advance. The most predictable component of sea level is a basin scale upward trend, predictable a decade in advance and primarily a response to increasing greenhouse gases. Significant additional predictability comes from multidecadal variations of the Atlantic Meridional Overturning Circulation (AMOC). While perfect model simulations show AMOC-related sea level predictability of 5-7 years, model biases and initialization uncertainties reduce the realized predictive skill to 3-5 years, depending on location. Overall, greenhouse gas warming and predictable AMOC variations lead to multiyear to decadal prediction skill for sea level along the U.S. East Coast. Such skill could have significant societal benefit for planning and adaptation.

[1] NOAA/Geophysical Fluid Dynamics Laboratory, Princeton, NJ, USA. [2] University Corporation for Atmospheric Research, Boulder, CO, USA.
✉email: Liping.Zhang@noaa.gov

Sea level change poses a serious threat to coastal communities[1]. The occurrence of high sea levels along the coast can cause catastrophic coastal flooding and inundation, threatening lives and infrastructure in the coastal regions[2–4]. Thus, sea level changes and associated coastal hazards are one of the most important societally relevant problems. Sea levels are impacted by many factors and can vary on broad time scales. On hourly to daily time scales, water level changes are primarily associated with the astronomical tide, waves, hurricanes, tropical cyclones, and extratropical storms[5–7]. On seasonal to multi-decadal time scales, sea level changes are usually linked to large scale ocean dynamics and climate variabilities[7–9]. In response to anthropogenic warming, sea levels have a secular rising trend over most oceans due to thermal expansion and the melting of land ice[7,10].

Over the North Atlantic Ocean, sea levels are substantially influenced by the wind, Gulf Stream and the Atlantic meridional overturning circulation (AMOC) on interannual and longer time scales[11–17]. The U.S. East Coast is a hot spot for the sea level change under current and future climates[18]. The long-term sea level change there was found to be ~two times faster than the global averaged rate. Dynamic sea level changes due to a weakening of AMOC are mainly responsible for this non-uniform change[15]. Due to geostrophic balance, a weakening of AMOC and northward Gulf Stream in the upper ocean results in a rising sea level along the western boundary of the Atlantic. This dynamic sea level rise (SLR) is then superimposed on the anthropogenic warming induced global mean SLR, eventually generating a higher-than-average SLR along the U.S. East Coast[15].

Given the high socioeconomic importance of sea level, particularly over the densely populated U.S. East Coast, there is a pressing need to forecast sea level on seasonal to decadal time scales to assist in mitigating impacts. Previous studies explored the seasonal prediction skill of sea level over global oceans using initialized climate model predictions[19,20]. They found a higher skill along the U.S. West Coast than that along the East Coast due to a stronger impact of El Niño-Southern Oscillation (ENSO) on sea level in the former region. However, prediction of sea level beyond seasonal time scales has received much less attention, yet such predictions may be beneficial for coastal infrastructure planning and investment. Many studies have demonstrated skillful decadal predictions for the AMOC and the North Atlantic upper ocean heat content that are relevant for sea level[21–25]. Thus, it is desirable to investigate the multiyear to decadal prediction of sea level. In this study, we use both diagnostic analysis and initialized decadal hindcasts to explore the multiyear to decadal sea level predictability/prediction over the North Atlantic region and the U.S. East Coast.

Results
North Atlantic Sea level predictability in control simulation.
We first use a diagnostic average predictability time (APT) method[26,27] applied to a preindustrial control simulation of the Geophysical Fluid Dynamics Laboratory (GFDL) SPEAR_LO model[28] (see Methods) to examine the North Atlantic Sea level predictability in a perfect model context. The APT is defined as the integral of predictability over all lead times and a linear regression model is adopted to estimate APT (see Methods). The APT analysis is similar to the empirical orthogonal function (EOF) decomposition, but here we decompose the predictability instead of variance.

We show in Fig. 1a–d the leading two predictable sea level components over the North Atlantic region. The most predictable component (APT1) has loadings of the same sign over the Labrador Sea and the western subpolar gyre region (Fig. 1a). The maximum occurs to the east of Newfoundland and extends to the U.S. East Coast, with substantial positive values north of Cape Hatteras. We also see sea level anomalies of the opposite sign in the eastern subpolar gyre, spreading southwestward to the west Atlantic. To the south, there are weak positive values within the 20°–30°N latitudinal band. This most predictable sea level component derived from the APT analysis shares many similarities with the dynamic sea level change in future climate change projections associated with a weakening AMOC, as well as in simulations that artificially weaken the AMOC through the application of anomalous freshwater fluxes to the subpolar gyre of the North Atlantic[15]. These results suggest that the predictability source may be closely linked to the AMOC. The associated APT1 timeseries shows low frequency variability with a period around 25–40 years (Fig. 1c), in agreement with the AMOC peak period in this SPEAR_LO control simulation[28]. The squared multiple correlation coefficient R^2 indicates that this APT1 component can be predicted approximately 7 years in advance (Fig. 1d). To understand the predictability source, we perform a lagged regression analysis of AMOC stream function against the APT1 time series (Fig. 1e). At a lag of 0-yr, the APT1 component corresponds to a weakened state of the AMOC. The lagged regressions from −16yr to 16 yr exhibit a clear evolution of the AMOC cycle, which highly resembles the AMOC internal variability in control simulation (Supplementary Fig. S1). Therefore, this leading predictable sea level component over the North Atlantic Ocean is largely associated with the mature phase (the time when the associated AMOC anomalies have maximum amplitude with either positive or negative sign) of a mode of internal variability in the North Atlantic that is associated with fluctuations of AMOC.

The physical processes are summarized as follows: the mature negative phase of AMOC is associated with weak deep-water formation over the Labrador Sea as well as a weak northward Gulf Stream and North Atlantic current. The entire ocean column in the western subpolar gyre has negative density anomalies, and thus has an expanded water column and positive sea level anomalies[15]. Changes in the geostrophic streamfunction are concurrent with steric sea level changes. The high sea level in the western part of the subpolar gyre further spins down the North Atlantic subpolar gyre, which inhibits upwelling of subsurface salty water and generates positive feedback. The Gulf Stream strength is reflected in the positive east-west sea level gradient across the U.S. East Coast and the interior Atlantic. Thus, to maintain the weak Gulf Stream and North Atlantic current, the sea level along the U.S. East Coast is higher and the sea level on the eastern side of the Gulf Stream/North Atlantic current is lower as required by the geostrophic balance[11,14–16] (Fig. 1a). The weak western boundary current is also accompanied with a weakening and southward shift of the subtropical gyre, which in turn leads to high sea level within the 20°–30°N latitude band. The opposite is also true for the mature positive phase of AMOC. The AMOC long persistence during the mature phase due to deep ocean memory leads to multiyear predictability of sea level over the North Atlantic region.

Next, we turn our attention to the second most predictable component of North Atlantic sea level (APT2, Fig. 1b). The second component is characterized by a tripole structure, with sea level anomalies of one sign near the Gulf stream path and sea level anomalies of the opposite sign to the north and south (Fig. 1b). The SLR near the Gulf Stream path exerts some impacts on the coastal region, but its influence is mainly confined south of Cape Hatteras. In addition, there are some weak SLR over the eastern subpolar gyre and south of 30°N. This component shares some similarities with the tripole sea level mode seen in the satellite altimetry that is characterized by a rapid acceleration of
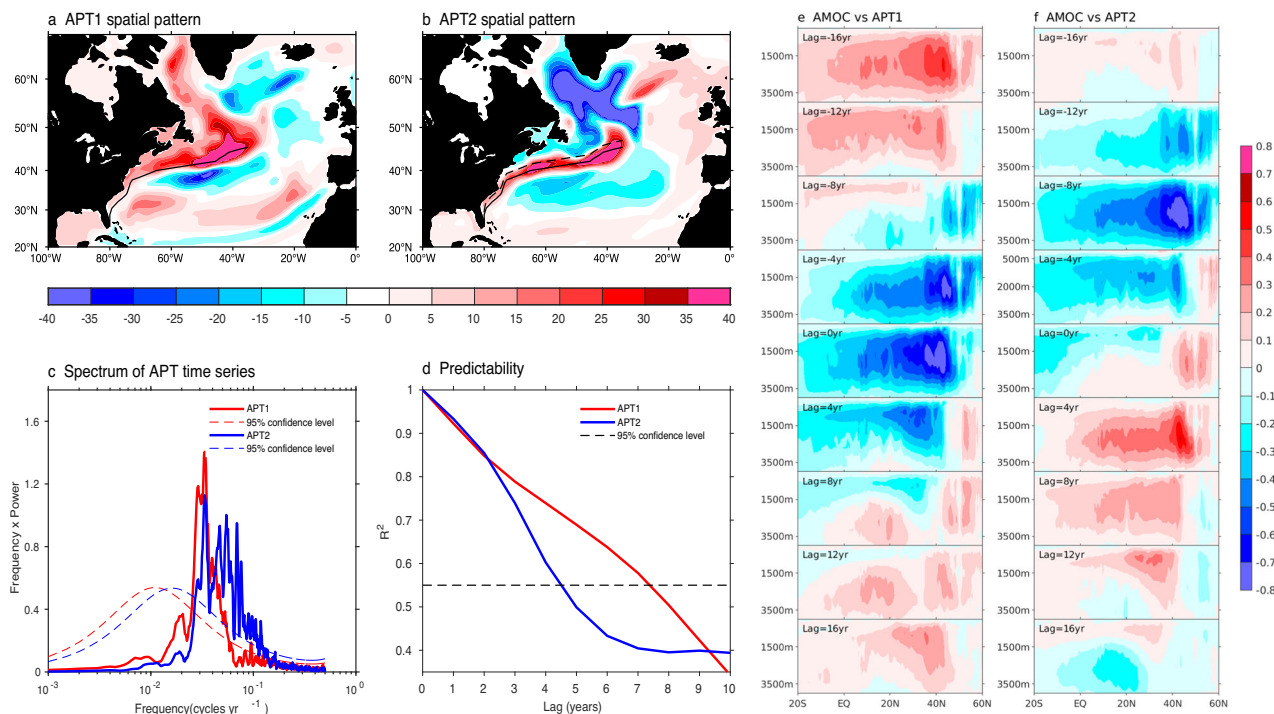
Fig. 1 North Atlantic sea-level predictability in SPEAR control simulation. a The leading predictable component (APT1) and **b** the second most predictable component (APT2) of North Atlantic Sea levels (mm) in SPEAR control simulation derived from the average predictability time (APT) analysis. The solid black lines in **a**, **b** denote the long term mean Gulf Stream path in model. For each latitude, the Gulf Stream path is defined as the longitude where there is a maximum of the zonal sea surface height gradient. The dash black line in **b** denotes the composited Gulf Stream path when the APT2 timeseries show positive values above 1. **c** Power spectrum of the associated APT1 and APT2 time series. The dash lines denote the 95% confidence level based on red noise null hypothesis. **d** Squared multiple correlation coefficients R^2. The dashed black line denotes the 95% confidence level estimated by Monte Carlo experiments. **e** Lagged regressions (−16 to 16 years) of AMOC stream function against the APT1 timeseries. **f** Same as **e** but for the regressions against the APT2 timeseries. Negative (positive) lags denote the AMOC leads (lags) the APT time series.

SLR over the U.S. Southeast Coast and Gulf Coast after 2010[29,30]. A further examination reveals that this APT2 component fluctuates on multidecadal timescales (Fig. 1c), but with decreased amplitude and higher frequency variabilities compared to APT1 and thus lower predictability. The R^2 shows the APT2 has a significant predictive skill up to 4 years (Fig. 1d). The lag 0-yr regression analysis reveals that the APT2 is associated with transitions between phases of the dominant pattern of AMOC internal variability (90° phase, Fig. 1f). The associated sea level pattern is largely contributed from the steric sea level component, particularly the thermosteric component (Supplementary Fig. S2a–c). When the AMOC transits from a mature negative phase to a neutral phase, the weak AMOC anomalies propagate southward with a slow advection speed due to the existence of the interior pathway of North Atlantic deep water[31], which is also accompanied with a northward shift of Gulf Stream path[32] (Fig. 1a). The associated northward heat transport anomalies lead to a heat divergence (convergence) nearby the subpolar region (Gulf Stream path) (Supplementary Fig. S2d–f), thus cooling (warming) and lowing (elevating) sea levels in the subpolar gyre (nearby the Gulf Stream path and U.S. Southeast Coast). Similar to the APT1, the long-time scales associated with the AMOC transition phase provide the source of the predictive skill of North Atlantic sea level on multiyear time scales. These analyses suggest that if we could adequately initialize the AMOC in a numerical forecast model, the future evolution of North Atlantic Sea level is potentially predictable.

North Atlantic Sea level prediction skill in initialized decadal hindcasts. We next explore whether the perfect predictability

described in the previous section can be translated to actual prediction skill in the SPEAR_LO decadal prediction system. Retrospective decadal hindcasts/forecasts system[21] were conducted with the SPEAR_LO model, with initialization from an observationally constrained reanalysis (see Methods). Previous work has demonstrated that the observed low frequency North Atlantic Oscillation (NAO) variations can drive multidecadal AMOC variabilities over the North Atlantic Ocean[33]. In the reanalysis, the atmosphere and SST were constrained by observations through strongly restoring to observations and reanalysis products. In this manner the ocean component of the coupled SPEAR model experiences a sequence of surface heat and momentum fluxes that are very close to observations. These quasi-observation boundary conditions then drive a very reasonable AMOC evolution in the reanalysis, which is highly correlated with the reconstructed AMOC fingerprints and the Rapid array observations[21]. Our reanalysis therefore provides a very useful AMOC initial condition for the decadal hindcasts/forecasts. We again apply the APT method to the set of retrospective decadal hindcasts/forecasts (see Methods) but use satellite observations of sea surface height to do skill verifications. Note that the sea level climatological variance and variance at different lead times required by the APT method can be obtained directly from hindcasts/forecasts and thus we don't need to adopt the linear regression model that was used in control simulation.

Figure 2 shows the most predictable components of sea level in the decadal hindcasts and their corresponding prediction skills. The prediction skill is estimated by correlating the timeseries of the components in the hindcasts and observations, where the observed timeseries were obtained by projecting the satellite
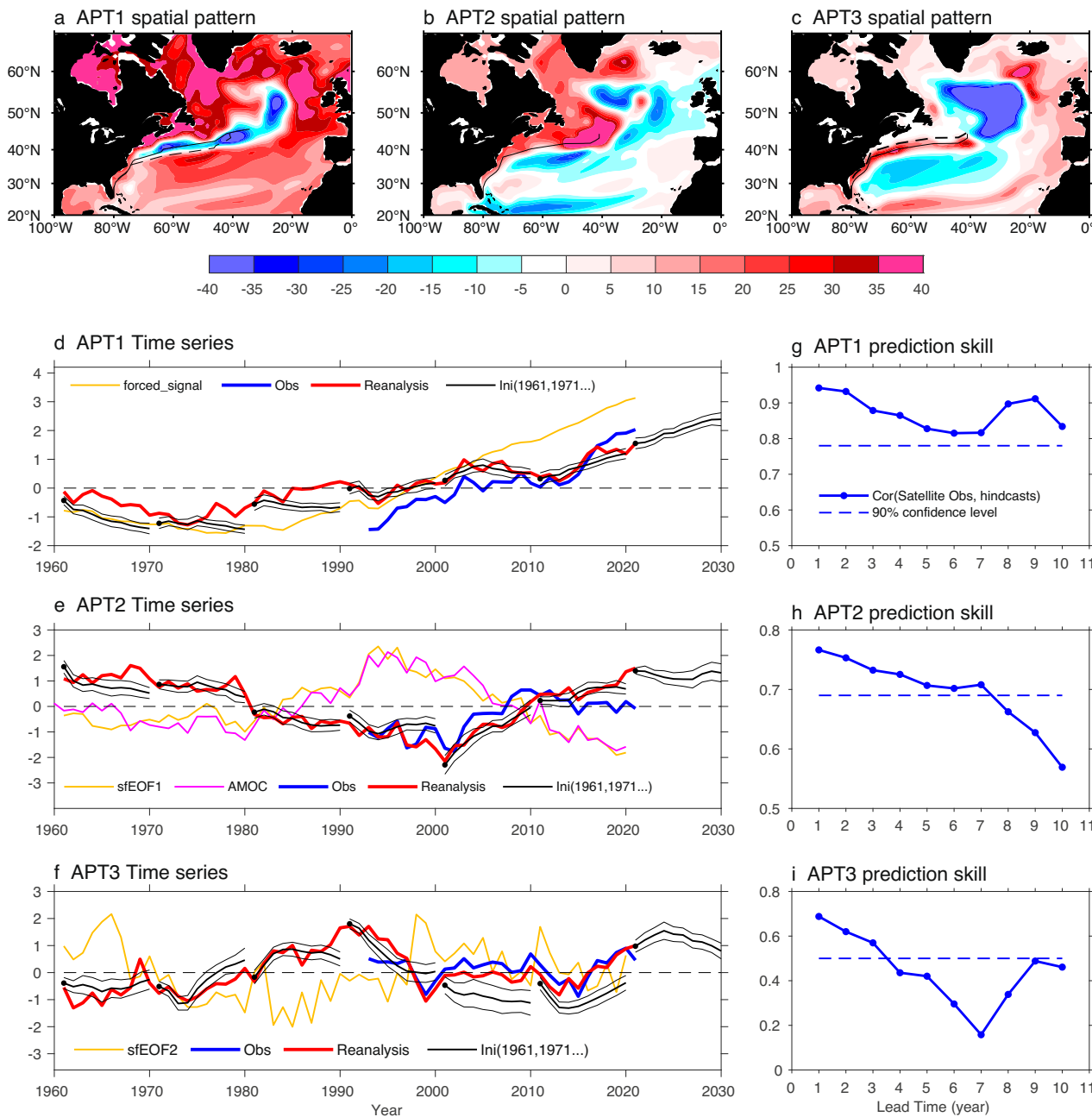
Fig. 2 The spatial structure, timeseries and prediction skill of the components that maximized the APT of sea level in the SPEAR initialized decadal hindcasts/forecasts. a The leading predictable component (APT1) of sea level (mm). **b** The secondary most predictable component (APT2). **c** The third predictable component (APT3). The black solid (dash) line in **a** denotes the Gulf Stream path averaged in the first (last) twenty years in SPEAR reanalysis. The black line in **b** and **c** denotes the long term mean Gulf Stream path in SPEAR reanalysis. For each latitude, the Gulf Stream path is defined as the longitude where there is a maximum of the zonal sea surface height gradient. The dash black line in **c** denotes the composited Gulf Stream path when the APT3 timeseries show positive values above 1.0. **d** The ensemble mean (black solid line) and spread (two thin black lines) timeseries as a function of lead times for the decadal hindcasts initialized on 1 January every ten years from 1961 to 2021. The red (blue) line is the timeseries for projecting the SPEAR_atm_sst_restore reanalysis (satellite sea surface height (SSH)) onto the APT1 component. The yellow line is the first principal component of sea level from the SPEAR large ensemble simulations using the signal-to-noise maximizing EOF analysis, which reflects the external forced signal. **e** Same as **d** but for the APT2 timeseries. The yellow line denotes the EOF1 timeseries of Atlantic stream function in reanalysis, while the magenta line denotes the AMOC index in reanalysis that is defined as the maximum stream function within 20°–60°N latitude band and below 500 m. **f** Same as **d** but for the APT3 timeseries. The yellow line denotes the EOF2 timeseries of Atlantic stream function in reanalysis. **g** Anomaly correlation between the APT1 timeseries in hindcasts and projected satellite observation timeseries as a function of lead times (blue solid line). The dash blue line denotes the 90% confidence level using a Monte Carlo method. **h** Same as **g** but for the APT2 timeseries. **i** Same as **g** but for the APT3 timeseries.

observation onto the spatial pattern of components. The leading predictable component (APT1) is characterized by a broad SLR over the North Atlantic basin except near the North Atlantic current path (Fig. 2a). The associated timeseries in hindcasts,

reanalysis and satellite observation all show an upward trend (Fig. 2d), indicating the important role of anthropogenic warming. This component can be predicted up to a decade ahead (Fig. 2g). To confirm the predictability source of the first

component, we derive the externally forced sea level variability over the North Atlantic region from SPEAR_LO large ensemble simulations (see Methods) using the signal-to-noise maximizing EOF analysis[34,35]. The externally forced sea level timeseries show an increasing trend and the forced spatial pattern highly resembles the APT1 component from the initialized SPEAR hindcast/forecast, with a spatial correlation up to 0.75 (Supplementary Fig. S3). This suggests that the most predictable component is primarily a response to external radiative forcing. The anthropogenic warming due to external radiative forcing warms the ocean, changes the ocean density, and thereby causes steric SLR[15,36]. The sea level fall in Fig. 2a is partly associated with a southward shift of the Gulf Stream path (Fig. 2a), which likely represents a compounding effect of the changes of AMOC and the wind driven circulation. In the west corner, some nonlinear factors such as the changes of Gulf Stream meanders may also play important roles. These need to be examined more in future work.

The second most predictable component in the initialized decadal hindcasts (APT2) highly resembles the APT1 component in control simulation (Figs. 2b and 1a). The projected APT2 timeseries in reanalysis show clear multidecadal variability, which is negatively correlated with the AMOC index as well as the EOF1 time series of Atlantic stream function in reanalysis (Fig. 2e), with correlation coefficients of -0.85 and -0.83, respectively. The EOF1 spatial pattern of Atlantic stream function in reanalysis corresponds to a mature positive phase of AMOC (Supplementary Fig. S4a, c). All these features indicate that the predictability source of this second predictable component is closely linked to the mature state of AMOC. Based on verification against the satellite projected time series, we find this component is predictable up to ~5 years in advance (Fig. 2h). The skill is a little bit lower than the perfect model skill seen in the control run presumably due to model biases and initialization uncertainties (Fig. 1d versus Fig. 2h). The third predictable component in decadal hindcasts (APT3) is characterized by a tripole pattern (Fig. 2c), which is very similar to the second most predictable component in control simulation (Figs. 2c and 1b). This component can be predicted ~3 years in advance (Fig. 2i). A close examination reveals that this component is highly correlated with the EOF2 time series of stream function in reanalysis that corresponds to a AMOC transition from one phase to an opposite phase (Fig. 2f and Supplementary Fig. S4b, d). Overall, the second and third predictive components in retrospective decadal hindcasts/forecasts are consistent with those from the control simulation. This further verifies that the AMOC can act as a predictability source to provide multiyear prediction skill for the long-time sea level change over the North Atlantic Ocean.

Multiyear to decadal predictions of sea level along the U.S. East Coast. As revealed by Fig. 2a–c, both the external radiative forcing and AMOC multidecadal variability exert great influence on sea level predictions along the U.S. East Coast. The radiative forcing provides a decadal predictability source for the long-term SLR over the whole U.S. East Coast, with increased impacts from south to north. The AMOC mature state contributes more to the coastal sea level predictability north of Cape Hatteras, while the AMOC transition state contributes more to sea level predictability south of Cape Hatteras. In the next section we focus on the U.S. East Coast and use the coastal tide gauge (TG) observations to verify our initialized decadal hindcasts (Fig. 3a).

To focus on low frequency sea level variabilities, we select TG stations over the U.S. East Coast where the data length is at least 50 years. The annual mean sea level timeseries displays an upward trend at all TG stations, largely due to the external

radiative forcing (Supplementary Fig. S5). After the linear trend is removed, the sea levels show substantial interannual fluctuations that are superimposed on multidecadal variability (Supplementary Fig. S5). On interannual timescales, the sea level variabilities have many similarities and are highly correlated north or south of Cape Hatteras (Supplementary Fig. S5)[37–39]. On multidecadal timescales, the sea level variabilities at the northeast TG stations (from the Halifax to Montauk stations) strongly covary with the projected APT2 time series in reanalysis (Supplementary Fig. S5), although the co-variability tends to attenuate from north to south. They are also negatively correlated with the AMOC index in the reanalysis, suggesting that the multidecadal sea level variations at these stations are very likely driven by the AMOC. At the New York and Atlantic city stations, the sea level timeseries become noisier and show much weaker variabilities on multidecadal timescales. For stations south of Cape Hatteras, the multidecadal sea level variations there are quite different, which is more correlated with the projected APT3 time series in reanalysis (Supplementary Fig. S5) and shows an acceleration of SLR after 2010[30], suggesting a potential linkage with the AMOC transition state. By taking all into account, we divide the U.S. East Coast into three sea level regimes: Northeast (north of New York), Mid-Atlantic (New York station; Atlantic City) and Southeast regimes (south of Cape Hatteras). The sea level composite is then calculated as the mean of annual sea level anomalies at all stations in each regime.

We show in Fig. 3 the sea-level composites from TG stations, initialized decadal hindcasts as well as their associated prediction skills. In the model, we search for the closest ocean grid to each TG station and thus obtain the corresponding hindcast timeseries by compositing sea levels in those ocean grids. The Northeast sea-level composite at TG stations shows a clear upward trend, largely due to the anthropogenic warming (Fig. 3b). This sea level rising trend can be predicted ~10 years in advance (Fig. 3c), in agreement with the satellite verification as displayed in Fig. 2g. The detrended sea-level composite at TG stations shows pronounced multidecadal variations, with high sea levels during 1945–1975, before 1920 and after 2010 and low sea levels during 1920–1940 and 1980–2010 (Fig. 3b). This timeseries is highly correlated with the projected APT2 timeseries and the AMOC index in reanalysis (Fig. 2e), with correlations up to 0.7 and −0.62, respectively. The internal sea level variations (see Methods) from initialized hindcasts at a lead time of 1-yr and 3-yr closely follow the sea level evolutions at TG stations (Fig. 3b). The anomaly correlation coefficient suggests that the Northeast sea-level composite has a prediction skill up to ~4 years (Fig. 3c). The skillful prediction is largely due to the successful capture of multidecadal variability of sea level in observations that is very likely driven by the AMOC. The detrended sea level prediction skill at each TG station is also examined over the Northeast regime. The prediction skill varies station by station, ranging from 1 year to 9 years (Supplementary Fig. S6). Overall, the prediction skill decreases from north to south, presumably due to the gradually attenuating ratio of multidecadal variabilities displayed in sea level timeseries (Supplementary Fig. S5). This north to south attenuating phenomenon is consistent with the influence of AMOC mature state on the coastal sea level predictability as revealed by APT analysis (Figs. 1a and 2b). This again indicates that the multiyear predictability source of sea level along the Northeast Coast of U.S. primarily arises from the AMOC mature state.

The Mid-Atlantic sea-level composite, again, shows a pronounced upward trend that can be predicted ~10 years in advance (Fig. 3d, e). However, the detrended sea level timeseries there are very noisy, with strong interannual variabilities in the most recent 20 years. This in turn leads to a disappearance of multiyear
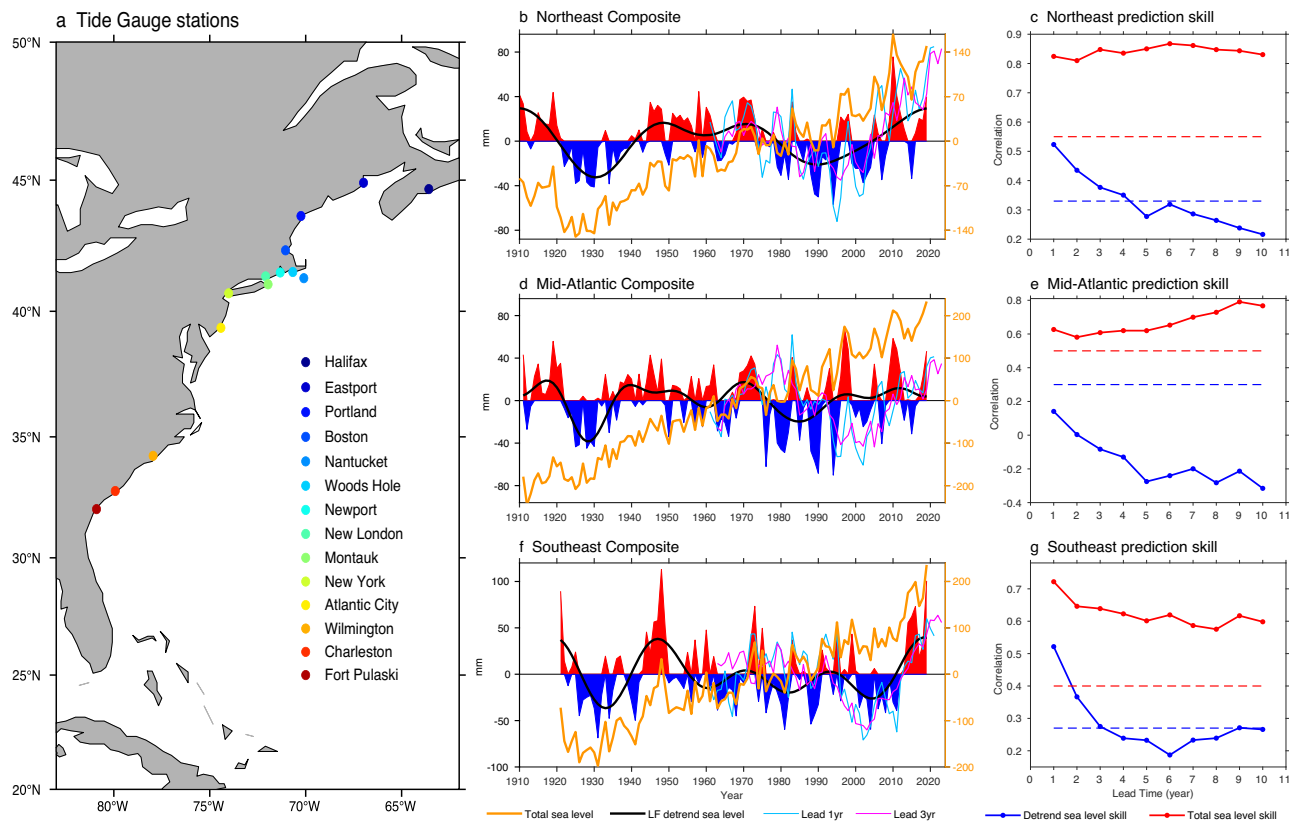
Fig. 3 Sea level multiyear to decadal prediction skill along the U.S. East Coast. a The locations of 14 tide gauge (TG) stations used in this study. The Northeast regime comprises stations north of the New York (Halifax to Montauk stations). The Mid-Atlantic regime includes the New York and Atlantic City two stations. The Southeast regime comprises stations south of Cape Hatteras (Wilmington to Fort Pulaski stations). **b** Timeseries of the Northeast sea-level composite (mm) from year 1910 to 2019. The yellow line (blue and red shading) denotes the total (linearly detrended) sea level anomaly timeseries at TG stations. The black line denotes the 11-yr low pass filtered timeseries of detrended TG sea levels. The light blue and magenta lines denote the internal sea levels in the initialized decadal hindcasts at a lead time 1 year and 3 years, respectively, where the forced signal is obtained using the signal-to-noise maximizing EOF analysis of the SPEAR large ensemble simulations and is then removed from the total sea level in model. **c** Shown are the anomaly correlation between the total (detrended or internal) sea level timeseries in the initialized decadal hindcasts and TG observations as a function of lead times denoted by the red (blue) line. The red and blue dash lines denote the 90% confidence level using a Monte Carlo method. **d**, **e** Same as (**b, c**) but for the Mid-Atlantic composite. **f**, **g** Same as **b**, **c** but for the Southeast composite.

prediction skill in this regime (Fig. 3e). We look further into each station and find the sea levels at the Atlantic City are noisier and less predictable than that at the New York station (Supplementary Fig. S5, 6). The multiyear sea level prediction skill reemerges when we move to the Southeast regime. As expected, the long-term trend of Southeast sea-level composite is predictable a decade in advance due to the external forcing (Fig. 3f, g). The detrended sea levels there have a prediction skill up to ~3 years. The initialized hindcasts at a lead time of 1-yr and 3-yr successfully capture the decadal to multidecadal sea level variabilities at TG stations, particularly in the most recent 30 years when there is a rapid SLR after 2010[29,30]. The sea level time series at all three southeast TG stations are highly correlated and their prediction skills are comparable (Supplementary Fig. S5, 6). The sea levels at the Southeast TG stations are more correlated with the projected APT3 timeseries than the APT2 timeseries in reanalysis, with correlations of 0.51 and 0.25, respectively. This suggests that the AMOC transition state plays a larger role in the sea level multiyear prediction skill in this regime, in agreement with the APT analysis shown in Figs. 1b and 2c.

Along the U.S. East Coast, the trend-like sea level skill verified by TG observations shows an increasing tendency from south to north (red lines in Fig. 3c, e, g), which is consistent with the APT analysis (Fig. 2a). This is because the external radiative forcing

not only induces a steric SLR that can be predicted on decadal time scales. It also weakens the AMOC, and the AMOC-related predictive skill is dominated by the AMOC mature state that shows increased skills from south to north along the U.S. East Coast (Figs. 1a and 2b). Adding these two factors together results in non-uniform trend-like sea level skills along the U.S. East Coast. In other words, the AMOC-induced SLR and its associated long memory facilitate the trend-like sea level skills over the U.S. Northeast Coast.

Summary and conclusion

In the present study, we assess the multiyear to decadal prediction skill of sea level over the North Atlantic regions by combining observations, multi-century control simulations with climate models, and initialized retrospective decadal hindcasts/forecasts. A statistical optimization APT method is used to identify the most predictable North Atlantic sea-level components. We identified three North Atlantic sea-level components that are skillfully predictable on multiyear to decadal timescales. The most predictable sea level component is characterized by a basin wide upward trend. This trend-like component is highly predictable at least 10 years ahead in SPEAR decadal hindcasts. The external radiative forcing is the main predictability source for the trend-like component. The second and third predictable sea level

components are related to the AMOC mature state and transition state, respectively. The former is characterized by sea level anomalies over the western subpolar gyre regions, with a maximum to the east of Newfoundland that extends to the U.S. East Coast, while the latter is featured by a tripole structure. These AMOC-related components are also clearly seen in control simulations, which have potential predictabilities up to 5–7 years in a perfect model context. In the initialized decadal hindcasts, the sea level skills are still maintained, with ~5 years for the second component and ~3 years for the third component after verified by satellite observations. The skill degradation likely results from model biases and uncertainties in initialization.

When we focus on the U.S. East Coast, the trend-like sea level skill due to external forcing tend to increase from south to north along the coast. This non-uniform skill is largely associated with the AMOC weakening in response to the external radiative forcing. The AMOC-induced dynamic SLR facilitates the trend-like sea level skill over the U.S. Northeast Coast. The detrended sea level skills along the U.S. East Coast are more related to the AMOC mature (transition) state in the Northeast (Southeast) regime, which can be predicted ~4 (3) years ahead when verified by TG observations. Overall, the AMOC long persistence due to subsurface ocean memory eventually reflects in sea levels along the U.S. East Coast, leading to multiyear to decadal prediction skills of sea level there.

Our initialized decadal forecasts indicate that the total sea level over the U.S. Northeast Coast will continue to rise in the next decade (Fig. 4a), since the external forcing and AMOC states all contribute positively to the SLR (Fig. 2d, e). The internal sea level component will continually have above normal anomalies for the next few years, although the amplitude of the anomalies will keep flat (Figs. 4b and 2e). It is also seen that the 10-yr sea level prediction initialized between 1995–2003 well captures the transition to multiannual high sea level events after 2005 (Fig. 4b). During these initialization years, the AMOC states were in mature positive phase (Fig. 2e), which are favorable for predicting the AMOC transition from positive to negative phases that are accompanied with a rising sea level trend. This again highlights a crucial role of the AMOC in the sea level prediction over the U.S. Northeast regime. However, we note that all hindcasts underestimate the extreme sea level high event during 2009–2010 (Fig. 4). This is because this extreme event is not only linked with the AMOC but also associated with the significant negative North Atlantic Oscillation (NAO) index[13] that is unpredictable on multiyear to decadal timescales.

In the current study, we demonstrate the multiyear to decadal predictability/prediction of sea level over the North Atlantic regions based on the GFDL SPEAR_LO decadal prediction system. We suggest that the multidecadal buoyancy driven AMOC variability is an important predictability source for the multiyear sea level prediction along the U.S. East Coast. In a future climate, the AMOC variability is very likely to decrease in response to global warming[40]. This may indicate that the sea level along the U.S. East Coast is less predictable on multiyear timescales in a future warming climate than the present day. This will be studied in our future work. In addition, we note that the SPEAR_LO does not include a land ice component, thus the SPEAR_LO cannot simulate the influence of Greenland ice sheet melt on the AMOC, sea level and geoid changes along the U.S. East Coast[41,42]. The SPEAR_LO underestimates the river discharges to the coastal seas as well[43,44]. These factors lead to a smaller magnitude of SLR over the U.S. East Coast in the model compared to the TG records, which eventually affects the trend-like sea level prediction skills. Moreover, the SPEAR_LO only has ~1° ocean resolution[28], therefore the Gulf Stream separation point has an obvious overshoot bias, and the coast and shelf break are not resolved very well[45,46]. The interannual sea level variabilities over the U.S. Northeast Coast in the model do not exactly covary with observations due to these factors, which can lead to prediction skill degradation of sea level. In addition, the SPEAR_LO does not simulate climate-unrelated factors, such as the land subsidence and land uplift that can change the relative SLR[47,48]. Ideally, predictions of multiyear to decadal sea level change over the North Atlantic regions should take all these factors into consideration. Although the SPEAR_LO has many shortages that may degrade the prediction skill, the key of the present paper is not to quantify the prediction skill, but rather to reveal the potential predictability sources. We hope the future model development and inter-model comparisons could address these and other shortages, therefore providing more accurate prediction information for better decision making and socioeconomic management.

Materials and methods

Observations. We use the sea surface height (SSH) from the Copernicus Marine Environment Monitoring Service[49], which is generated using satellite observations and is a mapped/interpolated product. The gridded version with a resolution of 0.25 degree is used in the present study. We also use the coastal sea level at tide gauge (TG) stations processed and distributed from the University of Hawaii Sea Level Center[50]. To focus on low frequency sea level variability, we use the annual mean sea level anomalies and correct the inverted barometer effect (IB) in tide gauge records to match the satellite observations. The IB is given by $IB = \frac{P_a - P_{gmean}}{\rho_0 g}$, where P_a is local sea level pressure, P_{gmean} is the global ocean averaged sea level pressure, ρ_0 is the sea water density and g is gravity. The sea level pressure dataset is from the 55-year Japanese Reanalysis (JRA-55)[51].

Model. The GFDL Seamless system for Prediction and Earth system Research (SPEAR) is used in the present study[28]. Here, we use the low ocean resolution version called SPEAR_LO. The ocean and ice components are from MOM6[52], which has a ~1° horizontal resolution (with refinements to 1/3° meridional resolution in the tropics) and 75 hybrid ocean layers in the vertical. The atmosphere and land components are from the AM4-LM4[53,54], which has a ~100 km horizontal resolution and 33 vertical levels.

We run a 4000-year control simulation of SPEAR_LO, with atmospheric composition fixed at preindustrial 1850 concentrations. The SPEAR_LO control simulation broadly captures the observed mean dynamic sea level features, including the high sea levels in the subtropical region and the low sea levels in the subpolar gyre region (Supplementary Fig. S7a, b). Compared to observation, the low sea levels in the subpolar gyre in model are more confined to the western part of the basin. The model also shows similar sea level variability over the North Atlantic midlatitude as the observation (Supplementary Fig. S7c, d). However, the sea level shows too weak (strong) variabilities in the west (east) of 55°W in model compared to observation, presumably due to weak eddy activities and recirculation in our coarse resolution model. It is worth noting that the SPEAR_LO doesn't have the land ice component, astronomical tide as well as climate-unrelated factors such as the land subsidence and land uplift. We also conduct large-ensemble simulations of SPEAR_LO, which cover the historical and 21st century periods[28,55] and are driven by both natural and anthropogenic forcings. The ensembles are comprised of 30 members, with each member initialized from different time of the control run that are 20 years apart in order to sample different phases of internal variability in the climate system.
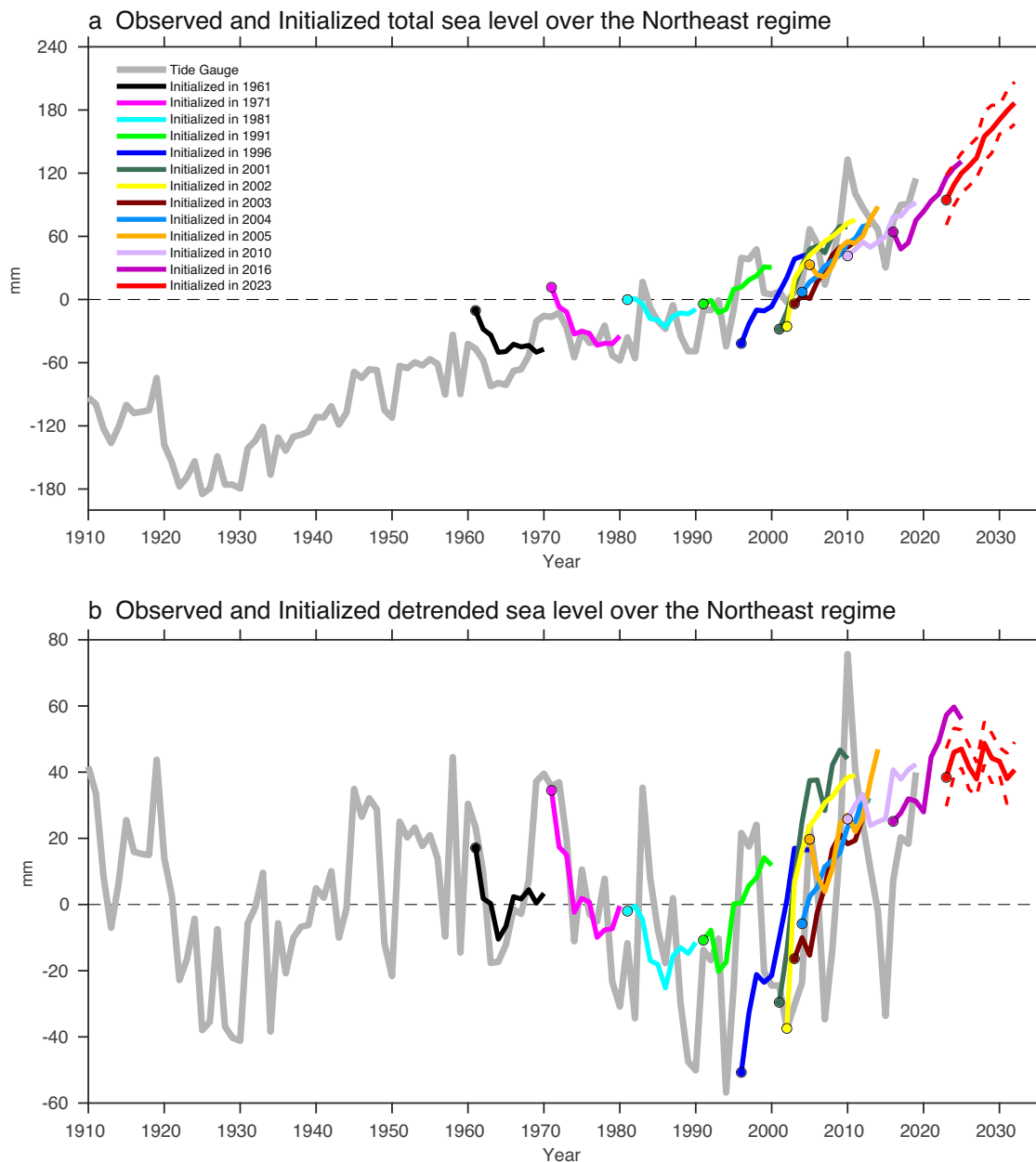
a Observed and Initialized total sea level over the Northeast regime

Tide Gauge
Initialized in 1961
Initialized in 1971
Initialized in 1981
Initialized in 1991
Initialized in 1996
Initialized in 2001
Initialized in 2002
Initialized in 2003
Initialized in 2004
Initialized in 2005
Initialized in 2010
Initialized in 2016
Initialized in 2023

b Observed and Initialized detrended sea level over the Northeast regime

Fig. 4 10-year predictions of sea level at different initialization years. a Total annual mean sea level time series at Northeast tide gauge stations (thick gray lines) and ensemble mean predicted 10-year sea level trajectories initialized between 1961 and 2023 (solid color lines). The dash red lines are the ensemble spread for the sea level prediction initialized in 2023 estimated by the one standard deviation of all members. **b** Same as **a** but for the detrended (internal) annually sea level time series. Unit is mm.

We developed a reanalysis for initializing retrospective decadal prediction system based on SPEAR_LO, which is named as SPEAR_atm_sst_restore[21,56]. In SPEAR_atm_sst_restore, the atmospheric component was restored toward the 55-year Japanese Reanalysis (JRA-55) on a 6-hourly time scale[51] and the SST within 60ºS-60ºN was restored to the Extended Reconstructed Sea Surface Temperature version 5 (ERSSTv5)[57]. The retrospective decadal hindcasts/forecasts using SPEAR_LO were then initialized from SPEAR_atm_sst_restore[21,56]. The hindcasts/forecasts have 20 members and were initialized on 1 January every year from 1961 to 2020 from different members of reanalysis and integrated for 10 years with the temporally varying historical forcings. The lead-time-dependent climatology is subtracted from hindcasts/forecasts before analysis in order to remove the systematic model drift.

APT methods. The average predictability time (APT) method is used to identify the most predictable components of annual mean North Atlantic sea-level in both control simulation and initialized decadal hindcasts[26,27]. The APT method was first proposed by DelSole and Tippett and was widely applied in many prediction studies across various timescales[58–60]. The APT is defined as twice the integral of predictability over all lead times:

$$\text{APT} = 2 \sum_{\tau=1}^{\infty} \left(1 - \frac{\delta_\tau^2}{\delta_\infty^2} \right), \tag{1}$$

where δ_τ^2 is ensemble forecast variance at lead time τ and δ_∞^2 is climatological variance. We then seek an inner product $\mathbf{q}^{\text{T}}\mathbf{x}$ to maximize APT, where $\mathbf{q}$ is a projection vector, $\mathbf{x}$ is the state vector and T denotes the transpose operation. Maximizing APT leads to

a generalized eigenvalue problem:

$$2 \sum_{\tau=0}^{\infty} (\textstyle\sum_{\infty} - \sum_{\tau})\mathbf{q} = \lambda \textstyle\sum_{\infty}\mathbf{q}, \tag{2}$$

where λ is the eigenvalue and is also the APT value. Thus, the APT decomposition is analogous to an Empirical Orthogonal Function (EOF) analysis, but here we decompose predictability instead of variance. For the initialized decadal hindcasts, we can easily get the climatological variance and forecast variance at different lead years since we have 20 ensemble members and 10 years prediction runs. For the control run, we only have a long single ensemble member, thus we adopt a linear regression model to estimate APT according to DelSole and Tippett[24,25]. The regression model is

$$\hat{\mathbf{x}}_{t+\tau} = \mathbf{L}_{\tau}\mathbf{x}(t) + \epsilon(t), \tag{3}$$

where $\mathbf{x}(t)$ represents the predictor at time t, $\hat{\mathbf{x}}_{t+\tau}$ is the predictand at time $t + \tau$, $\mathbf{L}_{\tau}$ is the regression coefficient and $\epsilon(t)$ is the residual term. Substituting (3) into the eigenvalue problem (5) leads to

$$\left(2 \sum_{\tau=1}^{\infty} \mathbf{C}_{\tau}\mathbf{C}_0^{-1}\mathbf{C}_{\tau}^T \right)\mathbf{q} = \lambda \mathbf{C}_0\mathbf{q}, \tag{4}$$

where $\mathbf{C}_{\tau}$ denotes the time lagged covariance matrix, $\mathbf{C}_0$ is the climatological variance, λ represents the eigenvalue and $\mathbf{q}$ denotes the projection vector, respectively.

When applying the APT method to control simulation, we first extract the leading 30 principal components of both the predictors and predictands. The resulting principal components are then split into half: The first half of data is called training data and are used to maximize APT in Eq. (4), while the second half is left for verification. The squared multiple correlation R_{τ}^2 is used to evaluate the potential predictability:

$$R_{\tau}^2 = \frac{\mathbf{q}^T\mathbf{C}_{\tau}\mathbf{C}_0^{-1}\mathbf{C}_{\tau}^T\mathbf{q}}{\mathbf{q}^T\mathbf{C}_0\mathbf{q}}. \tag{5}$$

We use the training data to calculate $\mathbf{q}$ and use the verification data to obtain the $\mathbf{C}_{\tau}$ and $\mathbf{C}_0$ two covariance terms. The slower decrease of R_{τ}^2 as a function of lead time, the larger potential predictability and vice versa. We use the Monte Carlo approach to test the statistical significance of APT[26,27]. If the APT value calculated from training data exceeds the 95% value from the Monte Carlo methods, the APT value from the training data will be significant at a 95% confidence level. We only show significant APT components in our article.

External forcing removal. To remove the effect of external radiative forcing, the linear trend at each TG station is removed before analysis. In the model, we remove the forced signal from the initialized decadal hindcasts at each lead time, where the external forcing is obtained from SPEAR_LO large ensemble simulations using the signal-to-noise maximizing EOF analysis[34,35]. We also tested other methods to remove the forced signal in model, such as the ensemble mean of large ensemble simulations and the linear trend. Similar prediction skills can be obtained for all these three methods. The signal-to-noise maximizing EOF technique extracts the forced signal by maximizing the ratio of signal variance (variance of ensemble mean) with respective to the noise variance (variance of member deviations from the ensemble mean) using large ensemble simulations.

Data availability

Code availability

References
1. Fitzgerald, D. M., Fenster, M. S., Argow, B. A. & Buynevich, I. V. Coastal impacts due to sea-level rise. *Annu. Rev. Earth Planet. Sci.* **36**, 601–647 (2008).
2. Kirwan, M. L. & Megonigal, J. P. Tidal wetland stability in the face of human impacts and sea-level rise. *Nature* **504**, 53–60 (2013).
3. Kirwan, M. L. et al. Overestimation of marsh vulnerability to sea level rise. *Nat. Clim. Chang.* **6**, 253–260 (2016).
4. Woodruff, J., Irish, J. & Camargo, S. Coastal flooding by tropical cyclones and sea-level rise. *Nature* **504**, 44–52 (2013).
5. Rahmstorf, S. Rising hazard of storm-surge flooding. *Proc. Natl. Acad. Sci. USA* **114**, 11 806–11 808 (2017).
6. Hirsch, M. E., DeGaetano, A. T. & Colucci, S. J. An East Coast winter storm climatology. *J. Clim.* **14**, 882–899 (2001).
7. Yin, J., Griffies, S. M., Winton, M., Zhao, M. & Zanna, L. Response of storm related extreme sea level along the US Atlantic coast to combined weather and climate forcing. *J. Clim.* **33**, 3745–3769 (2020).
8. Ezer, T. & Atkinson, L. P. Accelerated flooding along the US East Coast: On the impact of sea-level rise, tides, storms, the Gulf Stream, and the North Atlantic Oscillations. *Earth's Future* **2**, 362–382 (2014).
9. Ezer, T. Detecting changes in the transport of the Gulf Stream and the Atlantic overturning circulation from coastal sea level data: The extreme decline in 2009–2010 and estimated variations for 1935–2012. *Global Planet. Chang.* **129**, 23–36 (2015).
10. Tebaldi, C. et al. Extreme sea levels at different global warming levels. *Nat. Clim. Chang.* **11**, 746–751 (2021).
11. Little, C. M., Piecuch, C. G. & Ponte, R. M. On the relationship between the meridional overturning circulation, alongshore wind stress, and United States East Coast sea level in the Community Earth System Model Large Ensemble. *J. Geophys. Res. Oceans* **122**, 4554–4568 (2017).
12. Piecuch, C. G. et al. How is New England Coastal Sea Level Related to the Atlantic Meridional Overturning Circulation at 26ºN? *Geophys. Res. Lett.* **46**, 5351–5260 (2019).
13. Goddard, P. B., Yin, J., Griffies, S. M. & Zhang, S. An extreme event of sea-level rise along the northeast coast of North America in 2009–2010. *Nat. Commun.* **6**, 6346 (2015).
14. Yin, J. & Goddard, P. B. Oceanic control of sea level rise patterns along the East Coast of the United States. *Geophys. Res. Lett.* **40**, 5514–5520 (2013). (2013).
15. Yin, J., Schlesinger, M. E. & Stouffer, R. J. Model projections of rapid sea-level rise on the northeast coast of the United States. *Nat. Geosci.* **2**, 262 (2009).
16. Ezer, T., Atkinson, L. P., Corlett, W. B. & Blanco, J. L. Gulf Stream's induced sea level rise and variability along the U.S. mid-Atlantic coast. *J. Geophys. Res.* **118**, 685–697 (2013).
17. Levermann, A., Griesel, A., Hofmann, M., Montoya, M. & Rahmstorf, S. Dynamic sea level changes following changes in the thermohaline circulation. *Clim. Dyn.* **24**, 347–354 (2005).
18. Sallenger, A. H., Doran, K. S. & Howd, P. A. Hotspot of accelerated sea-level rise on the Atlantic coast of North America. *Nat. Clim. Chang.* **2**, 884 (2012).
19. Long, X. et al. Seasonal forecasting skill of sea-level anomalies in a multi-model predictionframework. *J. Geophys. Res.* **126**, e2020JC017060 (2021).
20. Long, X., Shin, S.-I. & Newman, M. Statistical downscaling of seasonal forecasts of sea level anomalies for U.S. coasts. *Geophys. Res. Lett.* **50**, e2022GL100271 (2023).
21. Yang, X. et al. On the development of GFDL's decadal prediction system: Initialization approaches and retrospective forecast assessment. *J. Adv. Model. Earth Syst.* **13**, https://doi.org/10.1029/2021MS002529 (2021).
22. Robson, J. I., Sutton, R. T. & Smith, D. M. Initialized decadal predictions of the rapid warming of the North Atlantic Ocean in the mid 1990s. *Geophys. Res. Lett.* **39**, L19713 (2012).
23. Smith, D. M. et al. Improved surface temperature prediction for the coming decade from a global climate model. *Science* **317**, 796–799 (2007).
24. Yang, X. et al. A predictable AMO-like pattern in the GFDL fully coupled ensemble initialized and decadal forecasting system. *J. Clim.* **26**, 650–661 (2013).
25. Yeager, S. G., Karspeck, A., Danabasoglu, G., Tribbia, J. & Teng, H. A decadal prediction case study: Late twentieth-century North Atlantic Ocean heat content. *J. Clim.* **25**, 5173–5189 (2012).
26. DelSole, T. & Tippett, M. K. Average predictability time. *Part I: Theory. J. Atmos. Sci.* **66**, 1172–1187 (2009a).

27. DelSole, T. & Tippett, M. K. Average predictability time. Part II: Seamless diagnosis of predictability on multiple time scales. *J. Atmos. Sci.* **66**, 1188–1204 (2009).

28. Delworth, T. L. et al. SPEAR – the next generation GFDL modeling system for seasonal to multidecadal prediction and projection. *J. Adv. Model. Earth Syst.* **12**, https://doi.org/10.1029/2019MS001895 (2020).

29. Volkov, D. L., Lee, S. -K., Domingues, R., Zhang, H. & Goes, M. Interannual sea level variability along the southeastern seaboard of the United States in relation to the gyre-scale heat divergence in the North Atlantic. *Geophys. Res. Lett.* **46**, 7481–7490 (2019).

30. Yin, J. Rapid decadal acceleration of sea level rise along the U.S. East and Gulf Coasts during 2010-2022 and its impact on hurricane-induced storm surge. *J. Clim.* **36**, 4511–4529 (2023).

31. Zhang, R. Latitudinal dependence of Atlantic meridional overturning circulation (AMOC) variations. *Geophys. Res. Lett.* **37**, L16703 (2010).

32. Zhang, R. Coherent surface-subsurface fingerprint of the Atlantic meridional overturning circulation. *Geophys. Rese. Lett.* **35**, L20705 (2008).

33. Delworth, T. L. et al. The North Atlantic Oscillation as a driver of rapid climate change in the Northern Hemisphere. *Nat. Geosci.* **9**, 509–512 (2016).

34. Ting, M., Kushnir, Y., Seager, R. & Li, C. Forced and Internal Twentieth-Century SST Trends in the North Atlantic. *J. Clim.* **22**, 1469–1481 (2009).

35. Ting, M., Kushnir, Y., Seager, R. & Li, C. Robust features of Atlantic multidecadal variability and its climate impacts. *Geophys. Res. Lett.* **38**, L17705 (2011).

36. Meehl, G. A. et al. How much more global warming and sea level rise? *Science* **307**, 1769–1772 (2005).

37. Boon, J. D. Evidence of sea level acceleration at U.S. and Canadian tide stations, Atlantic Coast, North. *Am. J. Coast. Res.* **28**, 1437–1445 (2012).

38. Ezer, T. Sea level rise, spatially uneven and temporally unsteady: Why the US East Coast, the global tide gauge record, and the global altimeter data show different trends. *Geophys. Res. Lett.* **40**, 5439–5444 (2013).

39. Andres, M., Gawarkiewicz, G. G. & Toole, J. M. Interannual sea level variability in the western North Atlantic: regional forcing and remote response. *Geophys. Res. Lett.* **40**, 5915–5919 (2013).

40. Cheng, J. et al. Reduced interdecadal variability of Atlantic meridional overturning circulation under global warming. *PNAS* **113**, 3175–3178 (2016).

41. Kopp, R. E. et al. The impact of Greenland melt on local sea levels: A partially coupled analysis of dynamic and static equilibrium effects in idealized water-hosing experiments. *Clim. Chang.* **103**, 619–625 (2010).

42. Bakker, P. et al. Fate of the Atlantic meridional overturning circulation: Strong decline under continued warming and Greenland melting. *Geophys. Res. Lett.* **43**, 12 252–12 260 (2016).

43. Durand, F. et al. Impact of Continental Freshwater Runoff on Coastal Sea Level. *Surv. Geophys.* **40**, 1437–1466 (2019).

44. Wada, Y. et al. Recent Changes in Land Water Storage and its Contribution to Sea Level Variations. *Surv. Geophys.* **38**, 131–152 (2017).

45. Chassignet, E. & Marshall, D. Gulf Stream separation in numerical ocean models. Ocean Modeling in an Eddying Regime. *Geophys. Monogr.* **177**, 39–61 (2008).

46. Gawarkiewicz, G., Ferdelman, T. G., Church, T. M. & Luther, G. W. Shelfbreak frontal structure on the continental shelf north of Cape Hatteras. *Cont. Shelf Res.* **16**, 1751–1773 (1996).

47. Nienhuis, J. H., Törnqvist, T. E., Jankowski, K. L., Fernandes, A. M. & Keogh, M. E. A new subsidence map for coastal Louisiana. *GSA Today* **27**, 60–61 (2017).

48. Karegar, M. A., Dixon, T. H. & Engelhart, S. E. Subsidence along the Atlantic coast of North America: Insights from GPS and late Holocene relative sea level data. *Geophys. Res. Lett.* **43**, 3126–3133 (2016).

49. Taburet, G. et al. DUACS DT2018: 25 years of reprocessed sea level altimetry products. *Ocean Sci.* **15**, 1207–1224 (2019).

50. Caldwell, P., Merrifield, M. & Thompson, P. Sea level measured by tide gauges from global oceans—The Joint Archive for sea level holdings, version 5.5. NOAA/National Centers for Environmental Information, accessed October 2018, https://doi.org/10.7289/v5v40s7w (2015).

51. Kobayashi, S. et al. The JRA-55 Reanalysis: General specifications and basic characteristics. *J. Meteorol. Soc. Jpn.* **93**, 5–48 (2015).

52. Adcroft, A. et al. The GFDL global ocean and sea ice model OM4.0: Model description and simulation features. *J. Adv. Model. Earth Syst.* **11**, 3167–3211 (2019).

53. Zhao, M. et al. The GFDL Global atmosphere and land model AM4.0/LM4.0: 1. Simulation characteristics with prescribed SSTs. *J. Adv. Model. Earth Syst.* **10**, 691–734 (2018a).

54. Zhao, M. et al. The GFDL Global atmosphere and land model AM4.0/LM4.0: 2. Model description, sensitivity studies, and tuning strategies. *J. Adv. Model. Earth Syst.* **10**, 735–769 (2018b).

55. Zhang, L. et al. Roles of meridional overturning in subpolar Southern Ocean SST trends: Insights from ensemble simulations. *J. Clim.* **35**, 1577–1596 (2022).

56. Zhang, L. et al. The relative role of the subsurface Southern Ocean in driving negative Antarctic Sea ice extent anomalies in 2016–2021. *Commun. Earth. Environ.* **3**, 302 (2022).

57. Huang, B. et al. Extended Reconstructed Sea Surface Temperature, Version 5 (ERSSTv5): Upgrades, validations, and intercomparisons. *J. Clim.* **30**, 8179–8205 (2017).

58. Yang, X. et al. Seasonal predictability of extratropical storm tracks in GFDL's high-resolution climate prediction model. *J. Clim.* **28**, 3592–3611 (2015).

59. Zhang, L., Delworth, T. L. & Jia, L. Diagnosis of decadal predictability of Southern Ocean sea surface temperature in the gfdl cm2.1 model. *J. Clim.* **30**, 6309–6328 (2017).

60. Jia, L. et al. Skillful seasonal prediction of North American summertime heat extremes. *J. Clim.* **35**, 4331–4345 (2022).

Acknowledgements

Author contributions

L.Z. and T.L.D. conceived the initial ideas. L.Z. designed the study, performed the analysis, and wrote the manuscript. T.L.D., X.Y., F.Z. and L.Z. lead the development of SPEAR decadal prediction system. All authors contributed to the improvement of the manuscript.

Competing interests

The authors declare no competing interests.

Additional information

Supplementary information The online version contains supplementary material available at https://doi.org/10.1038/s43247-023-01093-w.

Correspondence and requests for materials should be addressed to Liping Zhang.

Peer review information *Communications Earth & Environment* thanks the anonymous reviewer(s) for their contribution to the peer review of this work. Primary Handling Editors: Heike Langenberg and Joe Aslin. Peer reviewer reports are available.

Reprints and permission information is available at http://www.nature.com/reprints

Publisher's note Springer Nature remains neutral with regard to jurisdictional claims in published maps and institutional affiliations.